Large Ocean Worlds with High-Pressure Ices

Baptiste Journaux, Klara Kalousova, Christophe Sotin, Gabriel Tobie, Steve Vance, Joachim Saur, Olivier Bollengier, Lena Noack, Tina Rückriemen-Bez, Tim van Hoolst, et al.

Noname manuscript No.
(will be inserted by the editor)

Large ocean worlds with high-pressure ices

Baptiste Journaux · Klára Kalousová · Christophe Sotin · Gabriel Tobie · Steve Vance · Joachim Saur · Lena Noack · Tina Rckriemen-Bez · Tim Van Hoolst · J. Michael Brown · Olivier Bollengier · Andrew Thompson

Received: date / Accepted: date

Abstract Insert your abstract here. Include keywords, PACS and mathematical subject classification numbers as needed.

Keywords High pressure ices · Titan · Ganymede · Callisto · Exoplanets · Habitability

GUIDELINES: The guidelines for the chapters are max 25-30 pages with approx. 3500 characters per page (w/o spaces) or 4100 characters (w/ spaces). Therefore, each subsection should be approximately 6150 characters, including spaces.

Introduction (Journaux / All)

One unique and intriguing aspect of large ocean-worlds is the rising influence of pressure on their hydrosphere physical state. Pressure induced phase transitions is a crucial and long known effect inside Earth and other planetary bodies interiors. On larger bodies like Ganymede, Callisto and Titan, as its thickness of becomes larger, the hydrosphere's pressure can far exceed the one found at the bottom of Earth deepest oceans and rise up to Earth's lower crust - upper mantle range . This is the range at which pressure starts to play a major role into phase stability, as well as phase physical properties. The occurence of high pressure water ice polymorphs as well as other high-pressure phases and the higher pressure and temperature in their rocky mantle and possibly their iron cores are a few of the main aspects that differentiate large ocean-worlds with smaller water-rich bodies.

High-pressure ices in Ganymede, Callisto, and Titan offers the prospect of geophysical phenomena not occurring on Earth, at least not in water. From what

B. Journaux
Department of Earth and Space Sciences
University of Washington, Seattle, USA.

S. Author
second address

has been revealed by spacecraft missions—Voyager, Galileo, and Cassini, mainly—these similarly sized worlds differ in composition and have had drastically different thermal histories. The occurrence and geodynamic behaviors of ices II, III, V, and VI have affected the thermal evolution of these worlds. Processes in high-pressure ices also determine the conditions that may or may not permit life.

This chapter is covering the complex physical, thermodynamic and dynamical aspects rising from the existence of thicker hydrospheres containing high pressure ice polymorphs and the resulting effects of larger mantle and iron cores in large ocean-worlds.

1 State of the art on Ganymede/Callisto/Titan (Steve)

Section **lead**/contributors: **Steve**, Christophe, Joachim,

1.1 Induction at Ganymede and Callisto (Joachim)

The tilt of Jupiter's magnetic moment with respect to its spin axis causes time-periodic magnetic fields at Jupiter's moons. These time-variable fields generate in electrically conductive layers secondary magnetic fields. Observations of these secondary, i.e., induced magnetic fields, thus provide diagnostic information on the electrical conductivity structure in the interior (75; 150; 109). Because frozen water is a very poor conductor, measurements by the Galileo spacecraft near Europa, Ganymede and Callisto provided evidence for saline subsurface oceans (75; 100; 80; 150; 110). Magnetic field measurements by the Galileo probe at Ganymede were however non-unique due to Ganymede's internal dynamo with its unknown higher order moments (81). Observations of the oscillation amplitudes of Ganymede's auroral ovals with the Hubble Space Telescope could overcome the non-uniqueness issue and led to minimum conductivity of 0.09 S/m for an ocean located between 150 and 250 km depth (108). A recent study at Callisto (56) showed that induction in its ionosphere is exceptionally strong at Callisto and might be able to explain the observed magnetic field perturbations by the Galileo spacecraft. Thus the existence of an ocean within Callisto should be considered an open question based on the existing observational evidence.

This section focuses on the occurrence and properties of high-pressure ices in the large icy moons. The underlying spacecraft data interpretations and further details of the workings of these worlds are described in the chapter by Soderlund et al.

- This is what we currently know - review of the papers
- Ask ISSI graphic team for a figure of interior structures of different deep icy worlds

1.2 Occurrence of High-pressure Ices in the Solar System

A discussed below, convection within the ices should proceed near the solidus temperature, leading to melt at the high-pressure ice and rock interface, and within

Table 1 Properties of high-pressure ocean worlds

	Radius (km)	Density (kg m^{-3})	Moment of Inertia
Titan[a]	2574.73±0.09	1879.8±0.004	0.3438±0.0005
Ganymede[b]	2631±1.7	1942.0±4.8	0.3115±0.0028
Callisto[c]	2410.3±1.5	1834.4±3.4	0.3549±0.0042

[a](66; 64)
[b](111), revised from (4)
[c](1)

the upper parts of the high-pressure ice (27; 72). Briny fluids under pressure can have densities exceeding those of high-pressure ices and thus may occupy the interface between rock and ice (61; 67; 135) or between the different layers of high-pressure ice (68; 138). Dissolved ions incorporate into high-pressure ice VI (and possibly also in ice phases II, III, and V). The incorporation in ice VI, based on studies of RbI, is 3x that in ice Ih (68).

1.2.1 Titan

The climate cycle and lakes in Titan's hydrocarbon hydrosphere hide an icy lithosphere and thick water ocean. Titan's mean ice Ih thickness is interpreted from *Cassini-Huygens* data to be 50-200 km based on topography and admittance (59); less than 100 km based on shape, topography, and gravity (93); and 55-80 km based on the observed Schumann resonance (8). This entire range of thicknesses is consistent with an ice VI layer at the base of the ocean, atop a low-density silicate interior. If Titan's ice is indeed thin and if the ocean has a low salinity, high-pressure ices may be minimal or absent entirely. Among the large icy satellites, only Titan is expected to have only ice VI in the current era. Models of Titan's thermal evolution indicate that high-pressure ice formed in the most recent 2 Ga or even less (131).

1.2.2 Ganymede

Ganymede's intrinsic magnetic field participation in a tidal resonance with Io and Europa suggest it has experienced high heating. In the recent epoch of the ≈500 Myr surface age, high heat flux and ice Ih as thin as ∼10 km are in accord with the formation of grooved terrains on the surface (54). The tidal heating required for these may be negligible today (12). The thickness of the H_2O layer probably exceeds 800 km (141). Ice III forms at the base of the ocean and atop ices V and VI for a cold model Ganymede (≈ 1 mW^{-2} at the surface) with a high-salinity ocean containing 10 wt% of $MgSO_4$ (Fig. **??**). Warmer oceans within the likely limits of Ganymede's heat (14) can eliminate ices III and V, but even just after its formation Ganymede seems likely to have had some amount of ice V.

1.2.3 Callisto

The evidence for an ocean at Callisto is not as strong as the evidence for oceans in Ganymede and Titan. Callisto's bulk MoI is larger than that of Titan (Table 1)

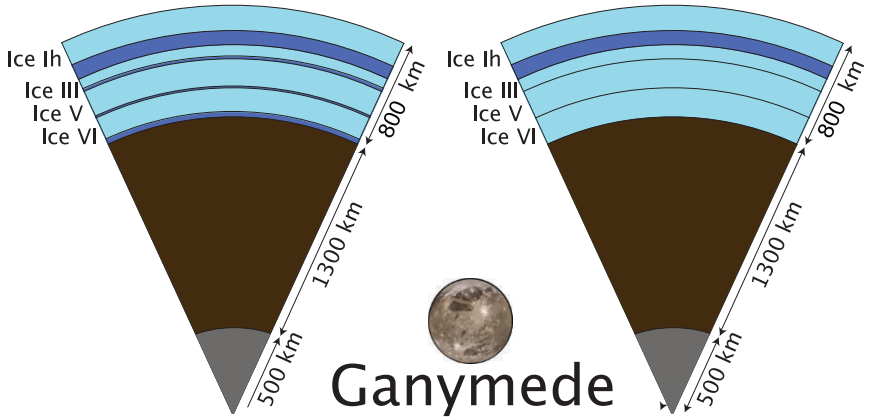

Fig. 1 Inferred internal structures for Ganymede. The radii where high-pressure ices form are computed based on published values of radius, bulk density, and gravitational moments of inertia (Table 1). Such solutions are non-unique, subject to the uncertainties in bulk properties, and to assumptions about the composition of oceans and minerals. The two depicted structures are consistent with additional geological and geophysical constraints on bulk heat flow and on the thickness of the ice Ih lithosphere. The existence of stable liquid regions between and beneath high pressure ices (left) depends on the transport of materials within the different ices. Modified from (141).

suggesting an even less differentiated interior (1) and a thinner hydrosphere. The existence of an ocean has been inferred from the detection of an induced magnetic field (74; 151), but the strength of the induced field might also be explained by plasma in the space environment near Callisto's surface (57). The value of the MoI as reported in Table 1 assumes hydrostatic equilibrium. If this assumption is not verified by future missions such as ESA's JUICE mission, then the error on the MoI could be very large (49) and Callisto may be more differentiated than presently thought.

The poor constraints on Callisto's density structure mean that an ocean there could be less than 250 km deep (Fig. 2—not so different from Europa—with little or no high-pressure ice. Or it could be more like Titan, with a seafloor at pressures approaching 800 MPa covered in ices V and VI. The inactive surface suggests weak or no differentiation; if Callisto has differentiated, it is difficult to conceive of how it would have cooled within a few hundred Myr to retain its cratering record. In either case, the fully stagnant upper lithosphere (91) suggests the ocean is nearly frozen and so has a near-eutectic composition. Buoyant ice II or III may be present, unless the ocean contains strong freezing suppressants such as ammonia or methanol.

Because of the greater uncertainties in the characteristics of Callisto's hydrosphere and the likelihood that Callisto has experienced less heating Ganymede, most studies of the dynamics of HP ice layers have focused on Ganymede and Titan.

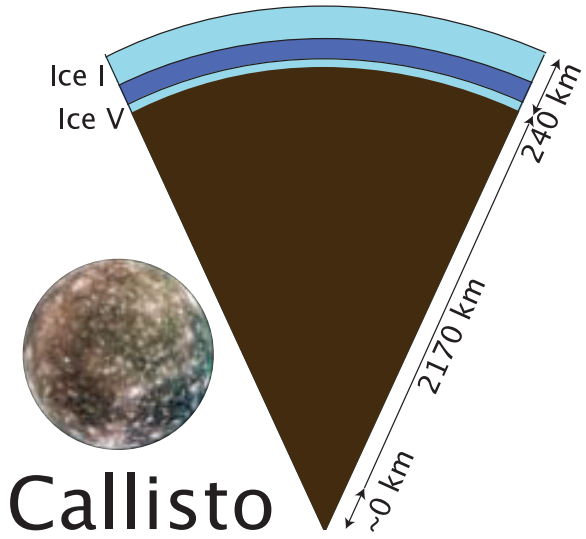

Fig. 2 Inferred internal structures for Callisto. Modified from (141).

1.3 Effects on Potential Habitability

The global fluxes of chemical energy must be understood in terms of a world's interior structure and evolution (140). Such a global picture is necessary for quantifying the types of life and amounts of biomass that might be supported (114). This is also required for interpreting any potential indications of life that might be found through in situ sampling, as, for example, by a lander on Europa's surface (55). In light of recent progress on the occurrence and potential stability of fluids within and underneath high-pressure ices (28; 72), it no longer seems to be the case that the presence of such ices impedes water rock interactions altogether. A more dire concern for the availability of chemical energy where high-pressure ices occur may be that the surface areas available for water-rock exchange are limited. High pressures at the water-rock interface (> 250 MPa) may force the elastic closure of fractures (139) and prevent tectonic opening (22).

In future exploration missions, geophysical measurements can reveal the properties of high-pressure ices in large ocean worlds. This creates the prospect for understanding geophysical phenomena analogous to processes on Earth—solid-state and heat pipe convection, multi-phase flow, porosity waves—in materials with different material behaviors from silicates. Geophysical measurements of processes in high-pressure ices are key to constraining heat flows and redox fluxes, and thus to identifying potential niches for life (141).

2 High-pressure physical chemistry of ices, aqueous solutions and relevant solids (Baptiste, Mike, Olivier)

Section **lead**/contributors: **Baptiste**, Mike, Olivier,

As described in the previous section, the pressures and temperatures expected in large icy moons hydrospheres (200−400K and 0−1.6 GPa) is such that high pressure ice polymorphs could be present, along with aqueous solutions, as well as hydrates and salt solid possibly. All of these phases have different structures and sometime very contrasted thermo-physical properties. Studying realistically the complex hydrosphere of water-rich planetary bodies is a challenging tasks as it requires to take into account the pressure, temperature and chemical (PTX) dependencies of all presents phases physical properties (e.g. aqueous solutions, ice polymorphs, salts and hydrates). These phases properties can be roughly classified as equilibrium thermodynamic properties (e.g. density, heat capacity, thermal expansivity, entropy, chemical potential) and transport properties (e.g. thermal diffusivity, viscosity, electrical conductivity). The first can be directly derived from underlying thermodynamic potential like the Gibbs free energy equation of state (EoS) [Brown, 2018]. These can be determined from experimental data or first-principle calculation (e.g. density functional theory, molecular dynamic modeling). Transport properties are not directly derivable from Gibbs-energy and therefore needs to be determined in-situ of from calculations, which are both challenging in that range of PT conditions.

This section aims at providing an overview of the known PTX dependency of important physical properties of relevant ice polymorphs, aqueous solutions and other solids found in the hydrosphere of ocean-worlds.

2.1 Water phase diagram at high-pressure

The water phase diagram, and more particularly its solid phases have been a rich and fruitful object of research since the discovery and description of its polymorphism in the beginning of the 20th century (18). There is, to this day, 18 crystalline polymorphs that have been characterized experimentally (92) and many tens of thousand predicted theoretically using exploratory first principle calculations(37). Many of these ice structures are stable or meta-stable above room pressure in a dense configuration (i.e. denser than liquid H_2O at similar along their melting curve). The more complex range of the phase diagram is arguably between 1 and 20.000 bar (2GPa), below room temperature where most of its stable and metastable polymorphs have been found (i.e. Ih, *Ic, II, III, *IV, V, VI, *IX, XI, *XII, *XIII, *XIV and XV; metastable phases noted with an asterisk) as well as a suite of clathrate hydrates structure and host molecules. This is the range of interest for icy moons' hydrospheres, and if metastable are theoretically possible in natural environments, it seems more likely that only the most stable phase will be present in their high pressure mantles. We will therefore focus this section on only the stable phases, ice Ih, II, III, V, VI for icy moons and VII and X for water-rich exoplanets.

Figure 3 represent the different stability fields of relevant stable high-pressure ices with the schematic region of interest for water-rich planetary bodies up to 3

GPa. Above that pressure cubic ice VII (and its possible variants VII' and VII") dominates the range of stability, with a gradual second order transition to ionic ice X above 50-100 GPa (60) and super-ionic ices above 2000K(92).

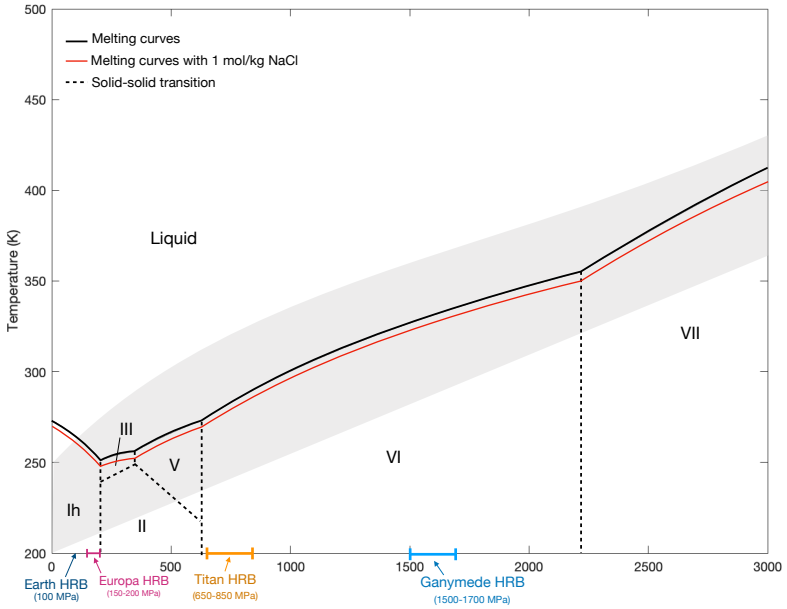

Fig. 3 Phase diagram of water showing stable ice polymorphs relevant to water-rich planetary body interiors. Melting curves from (144)and solid-solid phase transition from experimental data by (18; 19). The pressure range of the hydrosphere-rock boundary (HRB) is also reported for Earth, Europa, Titan and Ganymede.

2.2 Aqueous solutions at high-pressure.

2.2.1 Pure water thermodynamics

The physical and thermodynamic properties of aqueous solutions over this large range of pressure and temperatures is still a very active research area. The most advance model for liquid water thermodynamics was, up to recently, the IAPWS-95 formulation (143), that extended to 1GPa, with a large lack of data above 100 MPa leading to uncertainties at high pressures up to 20% in heat capacities, 0.2% in densities and 0.3% in sound speeds. New recent measurements have have enable to significantly extend the range of accuracy, and a new Gibbs energy representation based on local basis functions in the form of tensor B-splines enables easy and derivation of major equilibrium thermodynamic properties (including density ρ, heat capacities C_P & C_V, bulk moduli K_T & K_S, thermal expansivity

α, chemical potentials μ, sound speed, entropy S and enthalpy H) using Python, Matlab and Fortran function implementations (20); Bollengier et al., 2019]. This modular framework, called SeaFreeze, also has the advantage over many other previous thermodynamic code, to be able to represent chemistry dependence (e.g. solute concentration effects), as well as representing any solid phases and their equilibriums over the entire range of hydrosphere existing in our solar system.

Figure 4 left panel illustrate the variation in thermodynamic properties (ρ, α, C_P,K_T and sound speed) for pure water and 1 mol·kg^{-1} NaCl at 270, 300 and 350K extracted using SeaFreeze. This permits to illustrate how pressure has the largest effect overall on properties of aqueous solution that necessarily needs to be taken into account when integrating over the entire ocean. Temperature has a strong visible effect on density, thermal expansivity and heat capacity, but limited to negligible on bulk modulus and sound speed.

2.2.2 Aqueous solution thermodynamics

Quantifying the effects of chemistry at high pressure remains a more challenging endeavor as solvation interactions (and therefore the resulting effect on thermodynamic properties of solutions) strongly depends on the solute species and the pressure and temperature conditions. Therefore until molecular dynamic computation reach the adequate level of accuracy, one needs to experimentally measure these properties in-situ. Expected main planetary solutes includes salts species such as NaCl, $MgSO_4$ and Na_2SO_4, as well organics NH_3, CH_4 and CO_2. Here we only represent the effect of 1 mol·kg^{-1} dissolved NaCl (approximately twice sea-water concentration) for clarity, but other species, and ternary mixtures, will be included the SeaFreeze framework (e.g. $MgSO_4$, Na_2SO_4, $MgCl_2$, NH_3 and CO_2). Otherwise, scarce thermodynamic data and models currently exists for the pressure range found in large ocean worlds.

Thermodynamic representations exists for ammonia up to 2.3 GPa, including HP ices equilibria and based on experimental data (30) and for $MgSO_4$ (137; 136). Nevertheless, if the effects at low pressures have been extensively studied for most of these solutes, the >100MPa range remains largely unconstrained to this day (46; 117; 136; 142). For NaCl aqueous solutions, the results presented here are from the SeaFreeze Gibbs-every representation, based on sounds speed measurements under final development (Fig. 4, left panel) [see Bollengier et al. 2019 for approach details] . We can see from these results that the largest effect of chemistry change is visible for density, thermal expansivity and heat capacities. The bulk moduli and sound speeds remain less influenced by dissolved NaCl.

As reported in the previous section of this chapter, concentrated brines can become denser than the high pressure ices (61; 67; 135), potentially creating intermediate melt pockets at ice polymporphs interface or at the hydropshere-rock boundary (67; 135). It should be noted that concentration expected for density inversion to happen is generally above 1-1.5 mol/kg depending on the solute molar mass and the ice polymorphs density. These kind of concentrations are above the bulk amount expected in planetary oceans (152), but local pockets of dense brine could be possible.

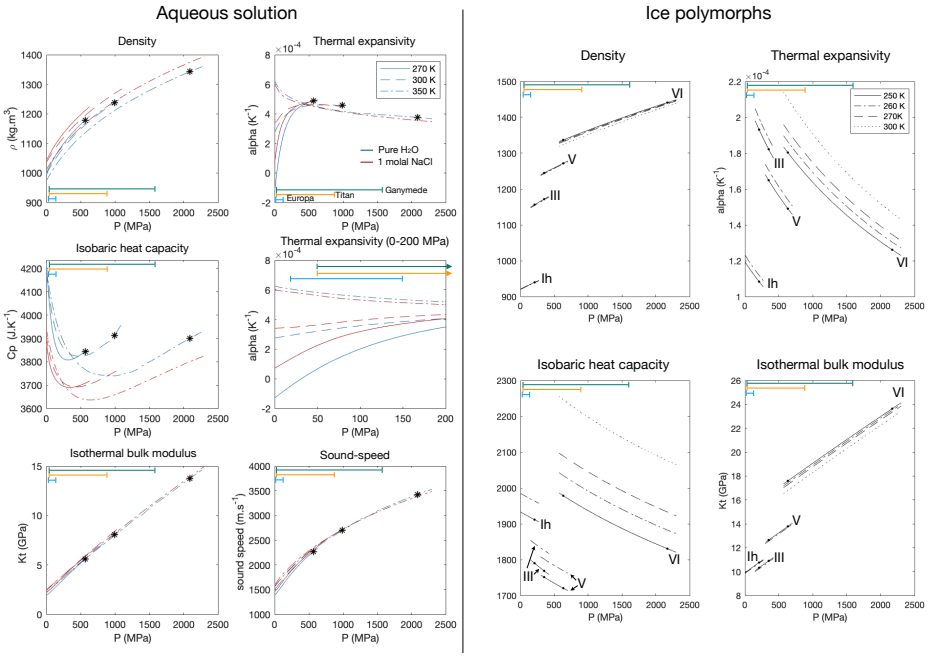

Fig. 4 Left panel: Aqueous solutions (pure H_2O and 1 mol·kg^{-1} NaCl) equilibrium thermodynamic properties evolution with pressure at 270, 300 and 350K extracted from the SeaFreeze framework (20); Bollengier et al., 2019]. High pressure ices freezing temperature are reported for pure water as dark asterisks, with ice V freezing at 270K and ice VI at 300 and 350 K. The estimated pressure range of icy moon hydrospheres are reported for Europa, Titan and Ganymede. Right panel: ice polymorphs thermodynamic properties evolution with pressure at 250 and 260K for all polymorphs and 270 and 300K for ice VI only.

2.3 High pressure ice polymoprhs

High pressure ice polymorphs have different crystallographic structures, hence contrasted thermodynamic and physical properties (see section for viscosities hereafter). The first discovery of ice polymorphism was reported by (126)and then further-explored by (18; 19). The pure water melting curves and solid-solid phase transitions (see Fig. 3) remain, to this day, mainly constrained by these old datasets (29; 33; 144).

2.3.1 Equilibrium thermodynamic properties

The gold standard for ice Ih equation of state is currently the Feistel and Wagner,)2006) parametrization (43) that provides a way to derive all important equilibrium thermodynamic properties from pressure and temperature derivatives of the Gibbs potential. High-pressure ices have remained sparsely studied until recently as they were only the interests of the physical chemistry community.

Melting curves and triple points of pure compound are usually described by Simon curves and parametrization for all the ices have been derived by (29) and (144). (29) also provides ad-hoc parametrization of chemical potentials and heat

capacities for ice Ih, II, III V and VI enabling to also compute solid-solid phase transitions. One issue with this representation is that the heat capacity is derived from (127)parametrization, itself based on an ill-chosen Debye model for the vibrational energy that cannot realistically reproduce molecular solids density of state, which tend to overestimate by more than 20% the heat capacity of high pressure ices [see Journaux et al. 2019].

Recent pressure-volume-temperature measurements by [Journaux et al. 2019] has enable to derive a full Gibbs energy representation for ice III, V and VI. The right panel in Figure 4 illustrate the evolution with pressure of the main equilibrium thermodynamic properties (density, thermal expansivity, heat capacity and isothermal bulk modulus), from 250 to 300 K, computed using the SeaFreeze package. Phase transition and the pressure variation have significant influence for all thermodynamic parameters represented here. The relativly small temperature range of interest for planetary hydrospheres represented here (250-300K) has an important effect on the thermal expansivity and heat capacity of all polymorphs. The density and bulk modulus remaining mainly influenced by pressure and phase transitions. Ice II is not represented here as its Gibbs energy representation is still investigated. General values can be found in (29; 30; 142).

It is also worth discussing the effect of chemistry on high pressure ices. Ice VI is the only high pressure polymorph with ice VII to have been investigated for salt incorporation (RbI as a NaCl analogue) (69). Ice VI seems to behave in a similar manner to ice Ih by mostly rejecting salts out of its structure during growth at equilibrium. Nonetheless, the very small amounts incorporated can have a significant effect on lowering its density (69). The possibility of solute incorporation of other expected planetary solute species (e.g. $MgSO_4$, $MgCl_2$, Na_2SO_4, etc.) for ice VI and if any incorporation is possible in other polymorphs still remains unconstrained to this day.

Ice VII has probably been the most studied after ice Ih due to its large stability field over 2 GPa and 300K. Furthermore, ice VII is a more complex phase as it seems to have several state of proton ordering (60) and is able to incorporate large amounts of ionic species while retaining its structure (82; 69; 16). Many pressure-volume-temperature data points and equations of state (EoS) are available for the pure H_2O. The most recent and common in the planetary science literature for ice VII up to 50GPa and below 1000K are the one from (10) and (83). For pressures above 50 GPa and temperature above 1000K, in the range interesting for ocean exoplanets, the evolution of thermodynamic properties and the location of phase transitions into plastic phase, ice X or super-ionic ice, remains an active field of experimental and theoretical study (47; 60; 92).

2.3.2 transport properties

TO FINISH

2.4 Other important solids

TO FINISH
salt hydrates

Clathrates

2.5 Final table with main properties

3 Dynamics of HP ice layer and exchange processes (Klara)

Section **lead**/contributors: **Klara**, Christophe
To include:

- HP ices Viscosity (Christophe)
- Dynamic and exchange processes through HP ices layers (Klara)

The main difference between the small to medium sized moons such as Enceladus or Europa, and the large moons Titan, Ganymede, and Callisto, is a much thicker hydrosphere in the case of large moons which results in the presence of a high-pressure ice layer between the silicate core and the deep ocean. Even though they have similar mass and radius, the large moons have different degrees of differentiation inferred from the values of the reduced moment of inertia (Table 1). As a result, Titan's hydrosphere is about 500 km thick (25), much thinner than Ganymede's which is about 800 km in thickness (135). In addition, Ganymede's gravity is higher than that of Titan. Combined with the hydrosphere thickness, this creates pressures at the silicates-hydrosphere interface twice as high on Ganymede (1.6 GPa) as on Titan (0.8 GPa). This has two important implications. First, in the case of Ganymede, most of the HP ice layer is composed of ice VI, while in the case of Titan, more phases are probably present - ice V if the HP ice layer is more than 80 km thick and ice III for HP ice layers over 250 km thick (Figure 5). Second, it indicates that Titan's ocean may have been in contact with the silicate core during a longer period of time compared to Ganymede (71).

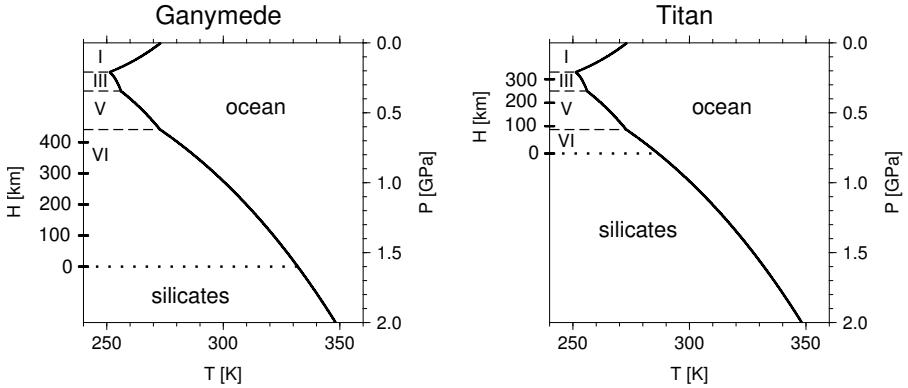

Fig. 5 Comparison of the P-T conditions within the HP ice layers of Ganymede (left) and Titan (right). The thick black line is the melting curve of pure ice (146; 145), the dashed lines indicate the phase transitions between the different ice phases, and the dotted line marks the interface between the hydrosphere and the silicate core. A possible range of HP ice layer thicknesses is indicated on the left axes.

The thermal/chemical evolution of the whole hydrosphere, including the HP ice layer, has been investigated by several authors for both Ganymede and Titan (77; 52; 115; 129; 44; 53; 11). In the majority of these studies, heat transfer through the HP ice layer was not explicitly treated and the temperature profile within the HP ice was assumed to follow the melting curve. Another approach is to describe the thermal state and heat transfer of the HP ice layer using scaling laws based on the instability of a hot thermal boundary layer at the interface with the silicates - this strategy was adopted by (53) for Titan and (101) for water-rich exoplanets.

As described above, several HP ice phases are likely present in the interior of large moons. To infer the effect of transitions between the different ice phases on convection in large satellites, (9) have performed a linear stability analysis considering a model consisting of two layers with the same viscosity and thickness. They found that an exothermic phase change can either impede or enhance the whole-layer convection, depending on the ice viscosity. For the endothermic transitions, they show that phase change always inhibits whole-layer convective overturn and tends to enforce two-layer convection. An extension of their approach was presented by (121) who found that taking into account different thickness and viscosity results in whole-layer convection for a much larger range of phase transitions parameters than previously thought.

Recently, Choblet et al. (28) performed numerical simulations of convection in the HP ice layer in 3D spherical geometry. They showed that melting can occur in the HP ice layer for a wide range of model parameters, especially at the top boundary with the deep ocean and possibly also at the bottom boundary with the silicates. In their model, they monitored the melt production and assumed that the generated melt is instantaneously extracted into the overlying ocean. Thus the matrix compaction associated with the volume change due to melting did not have to be taken into account.

To understand the fate of water within the HP ice layer, a numerical model must handle a mixture composed of two phases: solid ice and liquid water. The only studies on the topic have been conducted by Kalousova et al. (72; 70) for Ganymede and for Titan (71) using a 2D Cartesian model of convection of a two-phase mixture. This formalism allows a self-consistent treatment of both the melting process and the water flow within or through the convecting solid ice (depending on the ice permeability).

Independent of the particular treatment of melt, these studies have shown that the heat coming from the silicate core is transferred by convection through the HP ice layer and that the HP ice viscosity controls the layer dynamics. In the following, we summarize what is known about the HP ice viscosity before describing the results obtained with the two-phase models for Ganymede and Titan.

3.1 HP ice viscosity

Viscosity, the ratio of shear stress to strain rate, is a critical parameter that controls dynamics of the HP ice layer. For the very differentiated Ganymede that has a thick hydrosphere, the main HP ice phase is ice VI (Figure 5), while for Titan, which is less differentiated and has thinner HP ice layer, the main HP ice phases are ice VI and ice V.

The viscosity of HP ices has been measured by two groups. Sotin et al. (120) used a sapphire anvil cell to observe the deformation of ice VI at large values of shear stress (light blue rectangle in Figure 6). For values of 10^8 Pa, they have found a deformation rate of 10^{-2} s^{-1} (viscosity of 10^{10} Pa s, blue dots). They investigated the variations in a limited range of shear stress and temperatures close to the melting curve and found that the dependence of ice VI viscosity on the shear stress (value of the stress exponent) is small, which is interpreted as a result of temperature being close to the melting temperature. Extrapolation to typical convective shear stresses (gray rectangle) gives viscosities on the order of 10^{12} to 10^{14} Pa s, similar to the viscosities of ice I at its melting point, which are also very close to field measurements on glaciers (yellow rectangle) (62).

Another group led by Durham measured the viscosity of ice VI in a gas-medium high-pressure deformation rig (35; 34). The confining pressure was lower than that of Sotin et al.'s experiments (light red rectangle in Figure 6) and they found a much stronger stress dependence as expected at high values of shear stress and temperatures further from the melting point (red dots). Note however that their experimental strain-rates fall very closely to the extrapolation of the laboratory experiments of (120). Extrapolation of measurements of (34) suggests values of viscosity at the melting temperature on the order of 10^{17} to 10^{23} Pa s at typical convective stresses, which is orders of magnitude larger than values extrapolated from (120). Both studies (120; 35) suggest that viscosity is close to constant along the melting curve, which justifies the use of Arrhenius law (28; 72). Extrapolation from laboratory experiments (high stresses) to natural conditions (small stresses) can add large uncertainties, so numerical simulations usually consider a large range of viscosity values (28; 72; 70).

The relative viscosity of ice V compared to ice VI can be determined at the transition between the two phases. Figure 6 also shows the values of ice V viscosity (lines) at the triple point ice V - ice VI - water. (122) (blue lines) noticed that ice V is harder to deform than ice VI and that their viscosity ratio is close to two orders of magnitude at the experimental conditions. On the other hand, (35) found that ice V and ice VI have a similar plastic behavior. To accommodate this discrepancy in experimental results, Kalousova et al. (71) investigated viscosity ratios of up to 100 in their study tailored to Titan's HP ice.

3.2 Dynamics and exchange processes through the HP ices layers

The HP ice layer that is squeezed between the silicate core and the ocean is likely to be convecting according to the values of viscosity described previously. The presence of the above lying ocean implies that there is no cold thermal boundary layer (the temperature close to the ocean follows the melting curve) and thus the dynamics is driven by the upwelling thermal and compositional plumes that form at the bottom boundary. The results of simulations performed by (72) and (70; 71) have shown that the HP ice layer of thickness H can be divided into three parts (Figure 7): (1) a layer of temperate ice, i.e. ice whose temperature equals the melting temperature (T=T_m) at the top interface with the ocean - the thickness of this layer is H_t and melting always occurs in this layer, (2) a thick layer of convecting ice where some melting may occur depending on the efficiency of convection - its thickness is H_c, and (3) the bottom interface with the

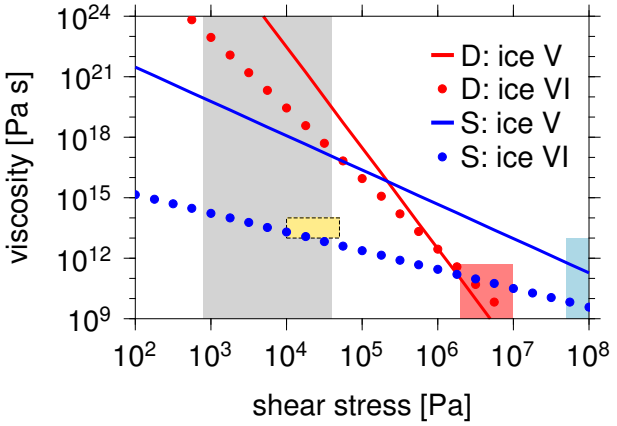

Fig. 6 Viscosity of ice VI (dots) and ice V (lines) as a function of shear stress measured by (120; 122) (blue) and (35; 34) (red). Light blue and light red rectangles indicate the experimental conditions, gray rectangle indicates the range of convective stresses, and yellow rectangle shows the range of viscosities measured in the terrestrial glaciers (62).

silicates where another temperate layer of thickness H_b may be present - melting may or may not occur at the silicates interface depending on the presence of this temperate layer. Based on the thermal structure of the HP ice layer, four different regimes of exchange between the silicates and the ocean were defined in (70) (cf. also Figure 7): (1) **direct exchange** (melting within all three regions, H_b, H_c, and H_t), (2) **indirect exchange** (melting at the bottom and top interfaces, H_b and H_t, but freezing within the convective domain H_c), (3) **limited exchange** (only limited melting at the bottom, $H_b \sim 0$, but melting within H_t), and (4) **no exchange** (no melting at the bottom, but melting within H_t). Note that no significant water is accumulated at the silicate interface.

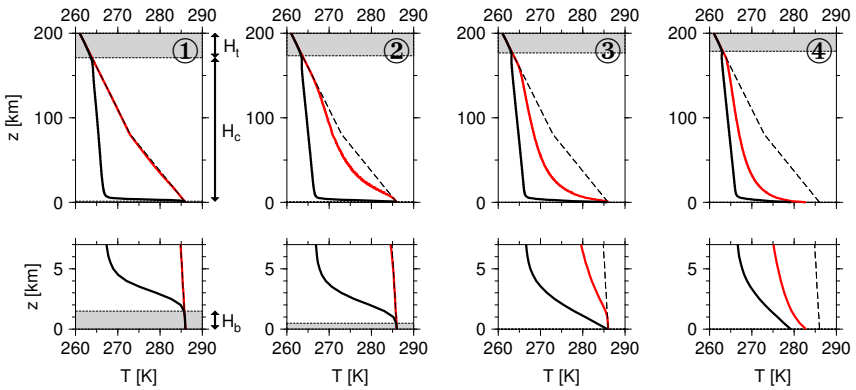

Fig. 7 Temperature profiles of each of the four exchange regimes (circled numbers). Maximum (red), horizontally-averaged (black), and melting (black dashed) temperature. Top and bottom temperate layers (gray). Bottom panels show bottom 7 km. Modified from the Supplementary Information of (71).

Table 2 Values of scaling parameters α and β (eq. 1) for Ganymede and Titan and different HP ice viscosities μ_0.

	Ganymede		Titan	
μ_0 [Pa s]	α	β	α	β
10^{14}	0.112	3.031	0.089	0.353
10^{15}	0.060	2.059	0.046	0.420
10^{16}	0.032	1.467	0.024	0.400

The occurrence or not of bottom melting depends on the efficiency of thermal convection in the HP ice layer - for high Rayleigh number, the heat transfer by solid-state convection is very efficient, the temperature at the silicates interface is below the melting temperature and thus no melting occurs - this corresponds to exchange regime #4. On the other hand, for small Rayleigh number, the heat transfer by convection is not very efficient, the whole layer warms and melting occurs at the silicates interface. This corresponds to regimes #1 and 2, while regime #3 is a transition between these two end members. Rayleigh number increases with the HP ice layer thickness H and decreases with the ice viscosity μ_i. Therefore, for a fixed viscosity, the increase in the HP ice layer thickness in time (crystallization of the sandwiched ocean) leads to increase of Rayleigh number and the transition from exchange regimes with bottom melting towards the regime without bottom melting. The exchange between the silicates and the ocean due to melting and water transport through the HP ice layer is thus more likely early in the moon's evolution when its HP ice layer is thin enough.

Based on the results of the numerical simulations, scaling laws were derived for Ganymede (70) and Titan (71). First, the occurrence of melt at the silicates interface was investigated and a scaling for a critical silicates heat flux q_s^c was found as a function of the HP ice layer thickness H which can be written as:

$$q_\mathrm{s}^\mathrm{c}[\mathrm{mW\ m^{-2}}] = \alpha H[\mathrm{km}] - \beta \tag{1}$$

Here α and β depend on the HP ice reference viscosity μ_0 and the particular values for Ganymede and Titan are given in Table 2. If the heat flux from the silicates is larger than the critical value q_s^c for a given HP ice layer thickness, melting occurs at the silicates interface. Figure 8 shows these scaling laws together with the estimate of the current heat fluxes from the silicate core assuming the CV and CI chondrites composition. Comparing these two informations, the critical values of HP ice layer thickness for the present-day melting at the silicate core can be inferred, depending on the ice viscosity. As discussed in Section 1.1.1, the thickness of Titan's icy crust is between 50 and 200 km and thus does not provide a strong constraint on the thickness of the HP ice layer that can be anything between 50 and 300 km in thickness. The scaling law predicts melting at the silicate interface for the lower bound of 50 km even for viscosities as low as 10^{14} Pa s. For the upper limit of 300 km, melting at the silicate interface would not occur unless the viscosity is larger than 10^{16} Pa s for CV abundances of radioactive elements and 10^{15} Pa s for CI abundances. For Ganymede, the presence of large impact craters suggests a thick icy crust which leads to a large thickness of the HP ice layer around 400 km suggesting that melting at the silicate interface is less likely than for Titan.

Scaling laws were also derived for the amount of melt produced at the silicates interface and the outflowing water velocity at the ocean interface. For both, the controlling parameter is the heat flux that comes from the silicate interior (70; 71). On the other had, the thickness of the top temperate layer H_t is mainly governed by the ice viscosity (70; 71).

The presence of melt at the interface between the silicates and the HP ice layer which facilitates the transfer of volatiles from the silicate core to the ocean is predicted by the two-phase models for large heat flux and thin HP ice layers. Ganymede's HP ice layer is believed to be thicker than Titan's for two reasons. First, Ganymede is more differentiated which leads to a thicker hydrosphere. Second, Ganymede's icy crust is likely thicker than Titan's based on the presence of large impact craters, which makes the ocean thinner and therefore the HP ice layer thicker. Consequently, melting at the HP ice/silicates interface is predicted to have occurred longer in Titan's interior and it may be ongoing.

One pending question is the effect of a cold ocean which freezes in the presence of salts. Preliminary results (71) suggest that the transfer to the ocean is limited by the presence of a cold boundary layer at the interface between the ocean and the HP ice layer. In addition, the exchange processes may be affected by the presence of salts in the melt produced at the interface between the silicates and the HP ice layer. Future work on this topic is required to fully appreciate the exchange between the silicate interior and the ocean through the HP ice layer.

Future missions such as the ESA JUICE mission for Ganymede and Callisto and the NASA Dragonfly mission, still in competition for the selection in the New Frontiers program, could provide additional constraints on the characteristics of the HP ice layer of these large icy moons.

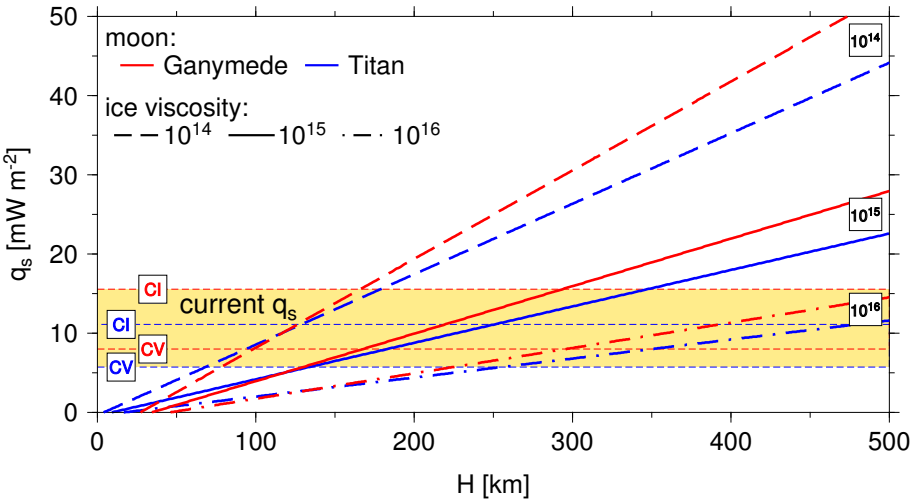

Fig. 8 The critical heat flux for the occurrence of bottom melting as a function of HP ice layer thickness (eq. 1) for Ganymede (red) and Titan (blue). Different line styles correspond to different ice viscosity. The yellow rectangle indicates the estimated present day heat flux from the silicate core of Titan (blue dashed lines) and Ganymede (red dashed lines) assuming CI and CV chondrites composition of the silicate interior.

4 Origin, differentiation and evolution

4.1 Accretion, impact-induced melting and ocean formation

Most of the icy moons of Jupiter and Saturn formed in a disk that was the outgrowth of the formation of planet itself. The conditions under which the giant planet formed therefore had a direct impact on the formation of their moons (e.g. 39; 107). The evolution of the circumplanetary disk is controlled by the accretion rate of the gas and dust from the surrounding solar nebula and the growth rate of the giant planet. A variety of models has been proposed to describe the evolution of the disk and growth of icy satellites from it (e.g. 23; 97; 98; 39; 107). The evolution of this disk determined the composition and architecture of the whole giant planet system as well as the final assemblage that led to the formation of regular icy moons. For instance, it has been proposed that the fact that Saturn has only one big moon (Titan) while Jupiter has four ones could be explained by difference in gas-dust infall from the solar nebula onto the subdisk (107). According to this model, Jupiter's formation and its subsequent migration into the disk may have resulted in a slower gas infall onto Saturn and subsequently to less available mass to accrete large icy moons.

A critical aspect concerns the way solids were incorporated into the disk. Different processes have been advocated (see for instance (39) and (24) for more detailed discussions): (1) direct transport of small particles into the disk with the inflowing gas, (2) ablation and gas drag capture of planetesimals orbiting the Sun through the gas-rich circumplanetary disk, (3) break-up, dissolution and recondensation of planetesimals in the extended envelope of the forming planet, (4) collisional capture of planetesimals. These various mechanisms result in difference in impactor size and velocity distribution, which has major consequences for the satellite accretion (94).

The size and velocity distribution of the impactors, as well as their composition, have probably varied in space and time within the subdisk (e.g. 104), which may explain the difference of composition between the icy satellites. Two reservoirs of primitive bodies may have contributed to the satellite growth: bodies in orbit around the planet, formed or captured within the circumplanetary disk, and bodies in orbit around the Sun, colliding directly with the growing satellite (e.g. 124). The contribution of each of these two reservoirs probably varied as the circumplanetary disk evolved. When the accretion sequence started, centimeter-sized planetocentric particles were probably pre-dominant, while kilometer-sized and larger bodies became more and more frequent during the late-stage of accretion.

By modeling the satellite accretion in 3D from a swarm of impactors of various size, Monteux et al.(94) tested the influence of impact size distribution on the thermal evolution of growing satellite. They showed that for satellites exceeding 1500-2000 km, surface melting can be avoided only if the satellite accreted relatively slowly ($>$ 1Myr) from small impactors ($<$ 1 km) and if the conversion of impact energy into heat is unrealistically inefficient ($<$ 1015%), confirming the first estimations of (7). However, as soon as a small fraction ($>$ 10%) of the impactor exceeds 1 km, global melting for large bodies like Titan or Callisto cannot

be avoided. Global melting results in the formation of an surface ocean in equilibrium with a massive primitive atmosphere generating by the release of volatile brought by the icy impactors (132; 89) (see Figure 9).

The post-accretional structure of a large icy moon like Titan or Ganymede thus consists of an inner undifferentiated ice-rock interior overlaid by a layer of sedimented rocks a thick liquid water ocean, resulting for melting of the icy impactor (78; 132). A primitive atmosphere potentially exceeding 10 bars can be maintained in equilibrium with the water ocean as long as the surface temperature exceeds the crystallization point. During this post-accretional period, the pressure at the base of the ocean is not large enough to lead to the formation of a high-pressure layer and the water ocean directly interacts with the sedimented rock layer, potentially promoting large-scale water-rock interactions and potential production of CH_4 and other gas compounds (50).

4.2 Heat budget and water-ice-rock segregation

During the early stages of the satellite history, in addition to impact heating, three main sources of energy may have contributed to the internal thermal budget: radiogenic heating, tidal heating associated with despinning and viscous heating due to ice-rock separation. Difference in accretion rate and/or heat sources may explain the difference in term of differentiation state between Ganymede, Callisto and Titan. Difference in the efficiency of heat and mass transfer from mixed ice-rock layer, owing to difference in post-accretional structure configuration, may further accentuate the differentiation dichotomy. These various processes which we briefly review in the rest of this section may explain the divergence in term of ice-rock segregation and internal melting between the three moons.

Impact heating results from the deposition of impactor kinetic energy during satellite accretion and subsequent intense bombardment periods. It therefore depends on the velocity and the mass of the impactor as well as the way kinetic energy is converted into heat. The impact creates a shock wave that compresses the satellite beneath the impact site. As shock compression is an irreversible process, the entropy below the impact site increases, leading to a temperature increase. Barr et al.(6) proposed that difference in impact energy received by Ganymede and Callisto during the late heavy bombardment event may potentially explain the dichotomy between two moons. As Ganymede is closer to Jupiter than Callisto, it is expected to experience twice as many impacts as Callisto. The impact velocity at Ganymede would have been also larger than at Callisto ($\sim$ 20 km.s^{-1} vs. $\sim$ 15 km.s^{-1}). This difference may have created a large scale melting of the outer envelop leading to runaway differentiation in the case of Ganymede, while impact-induced melting would have been more moderate at Callisto (7).

The heat sources may also significantly vary between these three large moons, due to difference in composition and orbital configuration. Internal heating due to short-lived radioactive isotopes (mainly ^{26}Al) probably does not play a role on these large moons. As the half-time of these short-lived elements is of the order

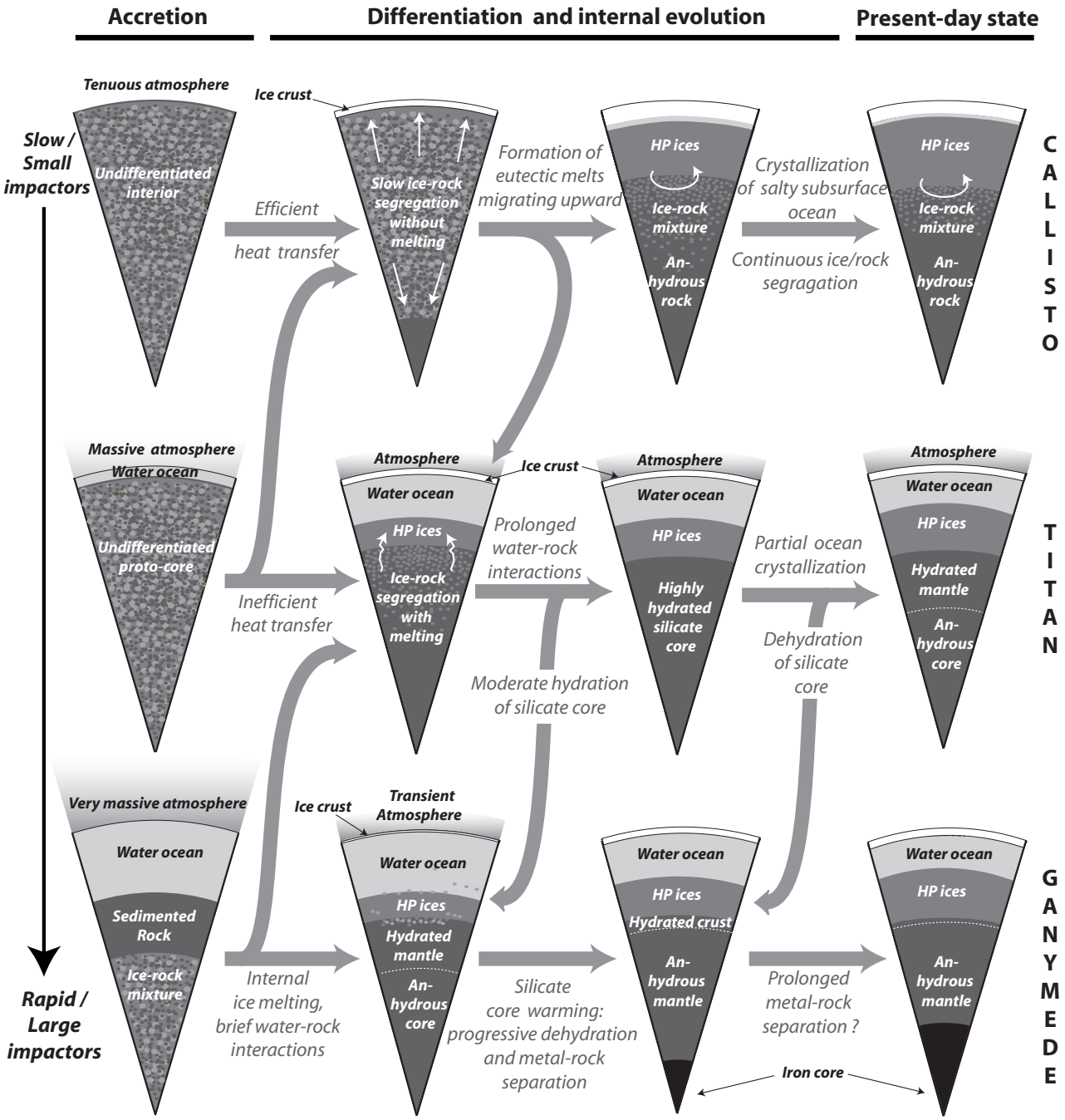

Fig. 9 Possible evolution scenarios for the interior of Callisto, Titan and Ganymede assuming different initial states. Depending mostly on the efficiency of heat transfer in the interior, different bifurcations in the evolutionnary path may have occurred explaining the present-day state of their interior. The interior structure shown here are just possible interior structures compatible with existing observational constraints. Existing data are, however, not sufficient to conclude with certitute concerning the differentiation state of these moons (Adapted from Tobie et al. (132))

.

of 1 million years, they are probably already negligible at the end of accretion of these big moons. The main heat source is then provided by the decay of long-lived radiogenic elements, mostly ^{40}K, ^{235}U during the first billion of years. Chondrites can be used to provide some estimate of the heat power generated by the radiogenic decay of the rocky phase in the moons. For Titan, carbonaceous chondrites, which are believed to be the dominant types of chondrites beyond Jupiter (84), are commonly assumed as good proxy of the rocky phase (45; 128; 50). For Jupiter's moons, LL-type ordinary chondrites have been proposed as possible rocky phase candidates (85; 86). Depending on the assumed chondritic composition, the initial radiogenic power may vary between 2.8 and 4.6 TW for Ganymede, and 1.9 and 3.2 TW for Callisto (63), a difference that could lead diverging evolution. For Titan, if we assume a composition dominated by CI chondrites, the total power should not exceed 2.5 TW (63).

Difference in tidal heating might also explain the dichotomy between these moons. Due to its closer distance to Jupiter and its interaction with Io and Europa through the Laplace resonance, Ganymede have likely experienced much more tidal heating than Callisto during its evolution (116; 13). In particular, it has been proposed by Malhotra(88) and Showman et al.(116) that the Galilean satellites may have passed through one or more Laplace-like resonances before evolving into the current Laplace resonance, resulting with prolonged periods with enhanced eccentricity and tidal dissipation in Ganymede (13; 15). By contrast, Callisto's eccentricity has probably remained rather small (0.007 at present) during its evolution, resulting in very small tidal forcing due to the distance to Jupiter (63). Tidal forces on Titan raised by Saturn are comparable to those experienced by Callisto. However, as Titan's eccentricity is much larger (0.0294 at present), this leads to large time variations of tidal forces, resulting in more tidal energy potentially dissipated. The existence of an elevated eccentricity for Titan in absence of orbital resonances similar to the Laplace resonance suggests that the eccentricity was larger in the past and that the present-day value is the remnant of a larger primordial value (130; 133). This implies that Titan may have experienced early during its evolution tidal heating rate comparable to Europa (130; 133). Simultaneously to accretion, the moons also experienced strong tidal dissipation resulting in despinning on the moons to tidally-locked spin-orbit resonance. Although the associated dissipation rate is very large, it lasted short periods of time, of the order of 100,000 years (63), resulting in a moderate temperature increase barely exceeding 25-50 K (132).

A last source of energy resulted from the release of gravitational energy associated to internal differentiation (48; 63; 132). The increase of temperature associated to change of gravitational energy between an initially homogeneous interior and a differentiated interior with a full separation of rock and ice phases is of the order of 100-150 K. If the ice-rock separation is fast enough ($< 0.5\,$Gyr), the dissipation of potential energy may induce runaway melting and thus may create a catastrophic differentiation, as it has been proposed for Ganymede (48; 78). If the differentiation process is slow and more gradual ($> 1\,$Gyr), the convective heat transfer should be able to transport this additional energy, preventing internal melting, as proposed for Callisto (99). O'rourke and Stevenson(102) showed, by using Titan as an example, that double-diffusive convection in ice/rock interior

can delay internal melting and ice/rock separation, but cannot prevent it, even if a reduced radiogenic power is assumed. This indicates that it seems very difficult to prevent full ice-rock separation, and therefore Callisto remains a mystery on this regard. We should, however, keep in mind that the process of ice-rock separation strongly depends on the rheology of ice-rock mixtures, which is poorly known at high pressure. Future experimental and modeling efforts are required to better understand the differentiation processes of large icy moons.

All along the differentiation process, internal melting may occur and also contribute to the efficiency of heat transfer, which has not been quantified so far. Melt migration is an efficient way to transport heat and to favor chemical exchanges. The composition of internal ocean has been likely conditioned by this leaching processes. Even though some studies have been focused on this topic, especially for Titan (38; 26; 45), lot of works still need to be done to understand the interplay between ice-rock segregation, fluid generation and transport and leaching processes.

4.3 Iron core formation and core-mantle-hydrosphere evolution

The existence of an iron core in the deep interior depends vitally on the degree of differentiation. As mentioned previously, Callisto and Titan seem to be only moderately differentiated, i.e. the rock+metal and ice phases may have been separated only incompletely (e.g. 3; 65). Furthermore both satellites lack an intrinsic magnetic field (73; 5), which is consistent with their partial differentiation. In contrast, Ganymedes low moment of inertia factor (MoI) (e.g. 2) and its intrinsic magnetic field Kivelson et al. (79) suggest a fully differentiated interior, i.e. further differentiation of the rock+metal primordial core into a metallic core and an overlying rocky mantle. Characterized by five flybys of the Galileo spacecraft, the magnetic field is predominantly dipolar with an equatorial surface field of 719 nT and a tilt away from the spin axis of 4^o(79). This unique magnetic field is most likely driven by a core dynamo, where kinetic energy is converted to magnetic energy. Core flows are likely driven by convection (e.g. 58) since libration-driven elliptical instability is likely absent (87) although precession-driven flows may still be possible. The existence of this magnetic field implies that the central iron alloy core must be at least partially liquid. The core size, however, is not well constrained with estimates ranging from one-quarter to one-third of the satellites radius (119). Core composition is similarly an open question with sulfur often assumed as the dominant light element (e.g. 113; 111) although other elements such as oxygen are also likely present (103).

Mckinnon (90) and Spohn et al. (123) show that, once ice and rock-metal phases are fully separated, radiogenic heating in the rock+metal phase is sufficient to raise the temperature to the Fe-FeS melting temperature. Such heating, however, may take several hundred million years assuming heat is not (or inefficiently) lost during the process (123). If enough melt is generated, it may permeate downwards to form a metal-rich core (e.g. 148). The slightly lower rock fraction of Callisto and Titan and therefore lower radiogenic heating compared to Ganymede

could be another reason for only partial differentiation of these two (111).

The thermal state of the satellites over time is strongly linked to radiogenic heating in the rocky part of the satellite as well as tidal heating. The latter, however, does not contribute significantly to the heat budget at present day for neither Callisto, Titan nor Ganymede. While tidal heating has never played an important role during Callistos history, it might have for Ganymede and Titan (e.g. 116; 118; 13; 134). Transfer of heat in the icy satellites is dominated by heat conduction and convection. Thermal convection occurs if the Rayleigh number – the ratio between diffusive and advective heat transport – exceeds a critical value. While convection is likely to occur in the putative liquid reservoirs of icy satellites like an ocean or a metallic core, it can be harder to achieve in the solid parts like the rocky mantle or the ice I crust (or high pressure ice phases). The onset of convection depends vitally on the viscosity, the thermal properties, and the size of the satellite. Different scenarios illustrating the basic mechanisms have been calculated by Ellsworth et al.(36) for the small Saturnian satellites. If convection occurs in the rocky mantle or the ice I crust it most likely operates in the so called stagnant lid mode due the strongly temperature-dependent viscosity of silicates and water ice (e.g. 112). Convection than takes place below a rigid shell across which heat is transported less efficiently via conduction.

If a metal core exists, which is the case for Ganymede, cooling of that core presents another heat source to the overlying rocky mantle and hydrosphere. Even though heat transport within the core is efficient due to convection, cooling of the core is limited to the amount of heat that can be extracted by the much more slowly convecting rocky mantle. The rocky mantle and metallic core are coupled via the temperature at the core-mantle boundary (cmb). If the core temperature has cooled sufficiently to drop below the melting point of the core alloy, the core will start to freeze. The latent heat released during freezing slows down cooling of the temperature at the cmb thereby temporarily increasing the heat flux into the mantle until heat transport in the mantle has adjusted to the new conditions (e.g. 125).

Based on experimental work on low-pressure Fe-FeS alloys, core differentiation in such small planetary bodies like Ganymede has been suggested to substantially differ from inner core growth (41; 40; 42; 32; 95; 96; 21). Instead of freezing from the inside out, the core likely solidifies from the top to the bottom (90; 58; 147). Thermal evolution models of metallic cores are important when it comes to estimating the power available to a potential dynamo. Given that Ganymede possesses an intrinsic, self-sustained magnetic field, considering the evolution of its metal-rich core is inevitable when it comes to global evolution models.

Thermal evolution models have largely focused on understanding how a satellite with such a small iron core could have an active magnetic field at present day. Although thermal convection has been considered (76), the majority of studies rely on thermo-compositional convection (58; 13; 105; 106). Here, compositional buoyancy is associated with the sinking of Fe snow assuming top-down core solidification for an iron-rich composition or with the upward flotation of solid FeS if the core is more sulfur-rich than the eutectic (17). Ruckriemen et al.(106), for

example, argue that both of these regimes can explain Ganymedes magnetic field, although dynamos driven by iron snow are generally young (less than 1 Byr) while FeS flotation dynamos can be up to 3.8 Byr.

Dynamo models simulating convection and magnetic field generation processes in the core are complementary to these studies. Zhan and Schubert (149) show that dynamo properties differ depending on the core crystallization regime and conclude that FeS flotation is most consistent with a dipole-dominated magnetic field, while Christensen et al. (31) show that convection driven by iron snow can reproduce Ganymedes observed dipole moment as well as its anomalously low quadrupole component. The contrasting conclusions of these studies is primarily a consequence of their different assumed source regions for compositional buoyancy (i.e. volumetric versus boundary origins) and the absence/presence of an outer stably-stratified layer in the model.

There are many directions for future work, given our limited understanding of core formation, evolution, and processes in icy ocean worlds. Future missions, in particular the ESA JUICE mission (51), will provide additional constraints on the core size and composition as well as magnetic field characteristics of Ganymede, while laboratory measurements that better characterize phase diagrams and transport properties in combination with thermal evolution and dynamo models would facilitate a more advanced interpretation of these measurements and answer fundamental questions such as what supplies the energy to drive the dynamo and for how long.

5 Discussion points and perspectives (Christophe)

Section **lead**/contributors: **Christophe**, Gabriel, Baptiste, Klara
To include:

- Does the presence of HP ice prevent the existence of hydrothermal vents ? (Steve)
- Exo-Ocean worlds (Lena, Baptiste, Christophe)
- Implications for large icy world habitability (All)
- Why are Ganymede Titan and Callisto so different ? (Steve + Christophe)
- What should be the future measurements (Gabriel, Tim)
  - Space mission (Gabriel, Tim, Joachim)tw
  - Experimental (Steve, Baptiste, Mike)

WRITE TEXT HERE

References

1. Anderson, J.: Shape, mean radius, gravity field, and interior structure of Callisto. Icarus **153**(1), 157–161 (2001). DOI 10.1006/icar.2001.6664. URL http://dx.doi.org/10.1006/icar.2001.6664

2. Anderson, J., Lau, E., Sjogren, W., Schubert, G., Moore, W.: Gravitational constraints on the internal structure of Ganymede. Nature **384**(6609), 541 – 543 (1996). URL http://dx.doi.org/10.1038/384541a0
3. Anderson, J., Schubert, G., Jacobson, R., Lau, E., Moore, W., Sjogren, W.: Distribution of rock, metals, and ices in Callisto. Science **280**(5369), 1573 – 1576 (1998). URL http://dx.doi.org/10.1126/Science.280.5369.1573
4. Anderson, J.D., Lau, E.L., Sjogren, W.L., Schubert, G., Moore, W.B.: Gravitational constraints on the internal structure of Ganymede. Nature **384**(6609), 541–543 (1996). DOI 10.1038/384541a0. URL http://dx.doi.org/10.1038/384541a0
5. Backes, H., Neubauer, F.M., Dougherty, M.K., Achilleos, N., André, N., Arridge, C.S., Bertucci, C., Jones, G.H., Khurana, K.K., Russell, C.T., et al.: Titan's magnetic field signature during the first cassini encounter. Science **308**(5724), 992–995 (2005)
6. Barr, A.C., Canup, R.M.: Origin of the Ganymede-Callisto dichotomy by impacts during the late heavy bombardment. Nature Geoscience **3**, 164–167 (2010). DOI 10.1038/ngeo746
7. Barr, A.C., Citron, R.I., Canup, R.M.: Origin of a partially differentiated Titan. Icarus **209**, 858–862 (2010). DOI 10.1016/j.icarus.2010.05.028
8. Béghin, C., Randriamboarison, O., Hamelin, M., Karkoschka, E., Sotin, C., Whitten, R.C., Berthelier, J.J., Grard, R., Simões, F.: Analytic theory of Titan's Schumann resonance: Constraints on ionospheric conductivity and buried water ocean. Icarus **218**(2), 1028–1042 (2012)
9. Bercovici, D., Schubert, G., Reynolds, R.T.: Phase transitions and convection in icy satellites. Geophysical Research Letters **13**(5), 448–451 (1986). DOI 10.1029/GL013i005p00448
10. Bezacier, L., Le Menn, E., Grasset, O., Bollengier, O., Oancea, A., Mezouar, M., Tobie, G.: Experimental investigation of methane hydrates dissociation up to 5GPa: Implications for Titans interior. Physics of the Earth and Planetary Interiors **229**, 144–152 (2014). DOI 10.1016/j.pepi.2014.02.001. URL http://www.sciencedirect.com/science/article/pii/S0031920114000260
11. Bland, M., Showman, A., Tobie, G.: The orbital–thermal evolution and global expansion of Ganymede. Icarus **200**(1), 207–221 (2009)
12. Bland, M.T., McKinnon, W.B.: Forming Ganymede's grooves at smaller strain: Toward a self-consistent local and global strain history for Ganymede. Icarus **245**, 247–262 (2015). DOI 10.1016/j.icarus.2014.09.008. URL http://dx.doi.org/10.1016/j.icarus.2014.09.008
13. Bland, M.T., Showman, A.P., Tobie, G.: The production of Ganymede's magnetic field. Icarus **198**, 384–399 (2008). DOI 10.1016/j.icarus.2008.07.011
14. Bland, M.T., Showman, A.P., Tobie, G.: The orbital–thermal evolution and global expansion of Ganymede. Icarus **200**(1), 207–221 (2009). DOI 10.1016/j.icarus.2008.11.016. URL http://dx.doi.org/10.1016/j.icarus.2008.11.016
15. Bland, M.T., Showman, A.P., Tobie, G.: The orbital thermal evolution and global expansion of Ganymede. Icarus **200**, 207–221 (2009). DOI 10.1016/j.icarus.2008.11.016
16. Bove Livia E., Ranieri Umbertoluca: Salt- and gas-filled ices under planetary conditions. Philosophical Transactions of the Royal Society A: Mathematical, Physical and Engineering Sciences

377(2146), 20180262 (2019). DOI 10.1098/rsta.2018.0262. URL https://royalsocietypublishing.org/doi/10.1098/rsta.2018.0262

17. Breuer, D., Rckriemen, T., Spohn, T.: Iron snow, crystal floats, and inner-core growth: modes of core solidification and implications for dynamos in terrestrial planets and moons. Progress in Earth and Planetary Science **2**(1), 1 (2015)
18. Bridgman, P.W.: Water, in the liquid and five solid forms, under pressure. Proceedings of the American Academy of Arts and Sciences **47**(13), 441–558 (1912). URL http://www.jstor.org/stable/10.2307/20022754
19. Bridgman, P.W.: The Phase Diagram of Water to 45,000 kg/cm2. The Journal of chemical physics **5**(12), 964–966 (1937). DOI 10.1063/1.1749971. URL http://link.aip.org/link/JCPSA6/v5/i12/p964/s1Agg=doi
20. Brown, J.M.: Local basis function representations of thermodynamic surfaces: Water at high pressure and temperature as an example. Fluid Phase Equilibria **463**, 18–31 (2018). DOI 10.1016/j.fluid.2018.02.001. URL http://www.sciencedirect.com/science/article/pii/S0378381218300530
21. Buono, A., Walker, D.: The fe-rich liquidus in the fe-fes system from 1bar to 10gpa. Geochimica et Cosmochimica Acta **75**(8), 2072–2087 (2011)
22. Byrne, P.K., Regensburger, P.V., Klimczak, C., Bohnenstiehl, D.R., Hauck II, S.A., Dombard, A.J., Hemingway, D.J.: The geology of the rocky bodies inside Enceladus, Europa, Titan, and Ganymede. In: 49th Lunar and Planetary Science Conference, p. Abstract #2905. Lunar and Planetary Institute, Houston (2018). URL http://www.lpi.usra.edu/meetings/lpsc2018/pdf/2905.pdf
23. Canup, R.M., Ward, W.R.: Formation of the Galilean Satellites: Conditions of Accretion. Astron. J. **124**, 3404–3423 (2002). DOI 10.1086/344684
24. Canup, R.M., Ward, W.R.: Origin of Europa and the Galilean Satellites, p. 59 (2009)
25. Castillo-Rogez, J.C., Lunine, J.I.: Evolution of Titan's rocky core constrained by Cassini observations. Geophysical Research Letters **37**(20) (2010)
26. Castillo-Rogez, J.C., Lunine, J.I.: Evolution of Titan's rocky core constrained by Cassini observations. Geophys. Res. Lett. **37**, L20205 (2010). DOI 10.1029/2010GL044398
27. Choblet, G., Tobie, G., Sotin, C., Běhounková, M., Čadek, O., Postberg, F., Souček, O.: Powering prolonged hydrothermal activity inside enceladus. Nature Astronomy **1**(12), 841–847 (2017). DOI 10.1038/s41550-017-0289-8. URL https://doi.org/10.1038/s41550-017-0289-8
28. Choblet, G., Tobie, G., Sotin, C., Kalousová, K., Grasset, O.: Heat transport in the high-pressure ice mantle of large icy moons. Icarus **285**, 252–262 (2017). DOI 10.1016/j.icarus.2016.12.002. URL http://dx.doi.org/10.1016/j.icarus.2016.12.002
29. Choukroun, M., Grasset, O.: Thermodynamic model for water and high-pressure ices up to 2.2 GPa and down to the metastable domain. The Journal of chemical physics **127**(12), 124506 (2007). URL http://www.ncbi.nlm.nih.gov/entrez/query.fcgi?db=pubmedcmd=Retrievedopt=AbstractPluslist$_uids$ = 128775486807678379$_related$: $tyh_zToG3xEJ$
30. Choukroun, M., Grasset, O.: Thermodynamic data and modeling of the water and ammonia-water phase diagrams up to 2.2 GPa for planetary geophysics. The Journal of Chemical Physics **133**(14), 144502–144502–13 (2010). DOI 10.1063/1.3487520. URL

http://link.aip.org/link/JCPSA6/v133/i14/p144502/s1Agg=doi
31. Christensen, U.: Iron snow dynamo models for ganymede. Icarus **247**, 248–259 (2015)
32. Chudinovskikh, L., Boehler, R.: Eutectic melting in the system fe-s to 44 gpa. Earth and Planetary Science Letters **257**(1), 97–103 (2007)
33. Dunaeva, A.N., Antsyshkin, D.V., Kuskov, O.L.: Phase diagram of H2o: Thermodynamic functions of the phase transitions of high-pressure ices. Solar System Research **44**(3), 202–222 (2010). DOI 10.1134/S0038094610030044. URL http://link.springer.com/10.1134/S0038094610030044
34. Durham, W., Stern, L.: Rheological properties of water ice—applications to satellites of the outer planets. Annual Review of Earth and Planetary Sciences **29**(1), 295–330 (2001). DOI 10.1146/annurev.earth.29.1.295
35. Durham, W., Stern, L., Kirby, S.: Rheology of water ices v and vi. Journal of geophysical research **101**(B2), 2989–3001 (1996)
36. Ellsworth, K., Schubert, G.: Saturn's icy satellites: Thermal and structural models. Icarus **54**(3), 490–510 (1983)
37. Engel, E.A., Anelli, A., Ceriotti, M., Pickard, C.J., Needs, R.J.: Mapping uncharted territory in ice from zeolite networks to ice structures. Nature Communications **9**(1), 2173 (2018). DOI 10.1038/s41467-018-04618-6. URL https://www.nature.com/articles/s41467-018-04618-6
38. Engel, S., Lunine, J.I., Norton, D.L.: Silicate interactions with ammonia-water fluids on early Titan. J. Geophys. Res. **99**, 3745–3752 (1994). DOI 10.1029/93JE03433
39. Estrada, P.R., Mosqueira, I., Lissauer, J.J., D'Angelo, G., Cruikshank, D.P.: Formation of Jupiter and Conditions for Accretion of the Galilean Satellites, p. 27 (2009)
40. Fei, Y., Bertka, C.M., Finger, L.W.: High-pressure iron-sulfur compound, Fe_3S_2, and melting relations in the Fe-FeS system. Science **275**(5306), 1621–1623 (1997)
41. Fei, Y., Li, J., Bertka, C., Prewitt, C.: Structure type and bulk modulus of fe3s, a new iron-sulfur compound. American Mineralogist **85**(11-12), 1830–1833 (2000)
42. Fei, Y., Prewitt, C., Mao, H., Bertka, C., et al.: Structure and density of fes at high pressure and high temperature and the internal structure of mars. Science (New York, NY) **268**(5219), 1892 (1995)
43. Feistel, R., Wagner, W.: A New Equation of State for H2o Ice Ih. Journal of Physical and Chemical Reference Data **35**(2), 1021–1047 (2006). DOI 10.1063/1.2183324. URL https://aip.scitation.org/doi/abs/10.1063/1.2183324
44. Fortes, A., Grindrod, P., Trickett, S., Vocadlo, L.: Ammonium sulfate on Titan: Possible origin and role in cryovolcanism. Icarus **188**(1), 139–153 (2007). DOI 10.1016/j.icarus.2006.11.002. URL http://dx.doi.org/10.1016/j.icarus.2006.11.002
45. Fortes, A.D.: Titan's internal structure and the evolutionary consequences. Plan. Space Sci. **60**, 10–17 (2012). DOI 10.1016/j.pss.2011.04.010
46. Fortes, A.D., Choukroun, M.: Phase Behaviour of Ices and Hydrates. Space Science Reviews **153**, 185–218 (2010). DOI 10.1007/s11214-010-9633-3. URL http://www.springerlink.com/index/10.1007/s11214-010-9633-3

47. French, M., Redmer, R.: Construction of a thermodynamic potential for the water ices VII and X. Physical Review B **91**(1), 014308 (2015). DOI 10.1103/PhysRevB.91.014308. URL http://link.aps.org/doi/10.1103/PhysRevB.91.014308
48. Friedson, A.J., Stevenson, D.J.: Viscosity of rock-ice mixtures and applications to the evolution of icy satellites. Icarus **56**, 1–14 (1983). DOI 10.1016/0019-1035(83)90124-0
49. Gao, P., Stevenson, D.J.: Nonhydrostatic effects and the determination of icy satellites' moment of inertia. Icarus **226**(2), 1185–1191 (2013). DOI 10.1016/j.icarus.2013.07.034. URL http://dx.doi.org/10.1016/j.icarus.2013.07.034
50. Glein, C.R.: Noble gases, nitrogen, and methane from the deep interior to the atmosphere of Titan. Icarus **250**, 570–586 (2015). DOI 10.1016/j.icarus.2015.01.001
51. Grasset, O., Dougherty, M.K., Coustenis, A., Bunce, E.J., Erd, C., Titov, D., Blanc, M., Coates, A., Drossart, P., Fletcher, L.N., Hussmann, H., Jaumann, R., Krupp, N., Lebreton, J.P., Prieto-Ballesteros, O., Tortora, P., Tosi, F., Van Hoolst, T.: JUpiter ICy moons Explorer (JUICE): An ESA mission to orbit Ganymede and to characterise the Jupiter system. Planet. Space Sci. **78**, 1–21 (2013). DOI 10.1016/j.pss.2012.12.002
52. Grasset, O., Sotin, C.: The cooling rate of a liquid shell in Titan's interior. Icarus **123**(1), 101–112 (1996)
53. Grindrod, P., Fortes, A., Nimmo, F., Feltham, D., Brodholt, J., Vočadlo, L.: The long-term stability of a possible aqueous ammonium sulfate ocean inside Titan. Icarus **197**(1), 137–151 (2008)
54. Hammond, N.P., Barr, A.C.: Formation of Ganymede's grooved terrain by convection-driven resurfacing. Icarus **227**, 206–209 (2014). DOI 10.1016/j.icarus.2013.08.024. URL http://dx.doi.org/10.1016/j.icarus.2013.08.024
55. Hand, K.P., Murray, A.E., Garvin, J.B., Brinckerhoff, W.B., Christner, B.C., Edgett, K.S., Ehlmann, B.L., German, C.R., Hayes, A.G., Hoehler, T.M., Horst, S.M., LUNINE, J.I., NEALSON, K.H., Paranicas, C., Schmidt, B.E., Smith, D.E., Rhoden, A.R., Russell, M.J., Templeton, A.S., Willis, P.A., Yingst, R.A., Phillips, C.B., Cable, M.L., Craft, K.L., Hofmann, A.E., Nordheim, T.A., Pappalardo, R.P., Team, t.P.E.: Report of the Europa Lander Science Definition Team. Tech. rep. (2017)
56. Hartkorn, O., Saur, J.: Induction signals from Callisto's ionosphere and their implications on a possible subsurface ocean. Journal of Geophysical Research (Space Physics) **122**(A11), 11 (2017). DOI 10.1002/2017JA024269
57. Hartkorn, O., Saur, J.: Induction signals from Callisto's ionosphere and their implications on a possible subsurface ocean. Journal of Geophysical Research: Space Physics **122**(11), 11,677–11,697 (2017)
58. Hauck II, S.A., Aurnou, J.M., Dombard, A.J.: Sulfur's impact on core evolution and magnetic field generation on Ganymede. Journal of geophysical research **111**(E9), E09008 (2006)
59. Hemingway, D., Nimmo, F., Zebker, H., Iess, L.: A rigid and weathered ice shell on Titan. Nature **500**(7464), 550–552 (2013). DOI 10.1038/nature12400. URL http://dx.doi.org/10.1038/nature12400

60. Hernandez, J.A., Caracas, R.: Proton dynamics and the phase diagram of dense water ice. The Journal of Chemical Physics **148**(21), 214501 (2018). DOI 10.1063/1.5028389. URL http://aip.scitation.org/doi/10.1063/1.5028389
61. Hogenboom, D.: Magnesium sulfate-water to 400 MPa using a novel piezometer: Densities, phase equilibria, and planetological implications. Icarus **115**(2), 258–277 (1995). DOI 10.1006/icar.1995.1096. URL http://dx.doi.org/10.1006/icar.1995.1096
62. Hudleston, P.J.: Structures and fabrics in glacial ice: A review. Journal of Structural Geology **81**, 1–27 (2015). DOI 10.1016/j.jsg.2015.09.003
63. Hussmann, H., Choblet, G., Lainey, V., Matson, D.L., Sotin, C., Tobie, G., van Hoolst, T.: Implications of Rotation, Orbital States, Energy Sources, and Heat Transport for Internal Processes in Icy Satellites. Space Sci. Res. **153**, 317–348 (2010). DOI 10.1007/s11214-010-9636-0
64. Iess, L., Jacobson, R.A., Ducci, M., Stevenson, D.J., Lunine, J.I., Armstrong, J.W., Asmar, S.W., Racioppa, P., Rappaport, N.J., Tortora, P.: The tides of Titan. Science **337**(6093), 457–459 (2012). DOI 10.1126/science.1219631. URL http://dx.doi.org/10.1126/science.1219631
65. Iess, L., Rappaport, N.J., Jacobson, R.A., Racioppa, P., Stevenson, D.J., Tortora, P., Armstrong, J.W., Asmar, S.W.: Gravity field, shape, and moment of inertia of Titan. Science **327**(5971), 1367–1369 (2010)
66. Jacobson, R.A., Antreasian, P.G., Bordi, J.J., Criddle, K.E., Ionasescu, R., Jones, J.B., Mackenzie, R.A., Meek, M.C., Parcher, D., Pelletier, F.J., et al.: The gravity field of the saturnian system from satellite observations and spacecraft tracking data. The Astronomical Journal **132**(6), 2520–2526 (2006). DOI 10.1086/508812. URL http://dx.doi.org/10.1086/508812
67. Journaux, B., Daniel, I., Caracas, R., Montagnac, G., Cardon, H.: Influence of NaCl on ice VI and ice VII melting curves up to 6GPa, implications for large icy moons. Icarus **226**(1), 355–363 (2013). DOI 10.1016/j.icarus.2013.05.039. URL http://dx.doi.org/10.1016/j.icarus.2013.05.039
68. Journaux, B., Daniel, I., Petitgirard, S., Cardon, H., Perrillat, J.P., Caracas, R., Mezouar, M.: Salt partitioning between water and high-pressure ices. Implication for the dynamics and habitability of icy moons and water-rich planetary bodies. Earth and Planetary Science Letters **463**, 36–47 (2017)
69. Journaux, B., Daniel, I., Petitgirard, S., Cardon, H., Perrillat, J.P., Caracas, R., Mezouar, M.: Salt partitioning between water and high-pressure ices. Implication for the dynamics and habitability of icy moons and water-rich planetary bodies. Earth and Planetary Science Letters **463**, 36–47 (2017). DOI 10.1016/j.epsl.2017.01.017. URL https://www.sciencedirect.com/science/article/pii/S0012821X17300237
70. Kalousová, K., Sotin, C.: Melting in high-pressure ice layers of large ocean worlds – implications for volatiles transport. Geophysical Research Letters **45**(16), 8096–8103 (2018). DOI 10.1029/2018GL078889
71. Kalousová, K., Sotin, C.: Dynamics of Titan's high-pressure ice layer. Earth Planet. Sci. Lett. p. submited (2019)
72. Kalousová, K., Sotin, C., Choblet, G., Tobie, G., Grasset, O.: Two-phase convection in Ganymede's high-pressure ice layer — implications for its geological evolution. Icarus **299**, 133–147 (2018). DOI 10.1016/j.icarus.2017.07.018. URL http://dx.doi.org/10.1016/j.icarus.2017.07.018

73. Khurana, K., Kivelson, M., Russell, C., Walker, R., Southwood, D.: Absence of an internal magnetic field at callisto. Nature **387**(6630), 262 (1997)
74. Khurana, K., Kivelson, M., Stevenson, D., Schubert, G., Russell, C., Walker, R., Polanskey, C.: Induced magnetic fields as evidence for subsurface oceans in Europa and Callisto. Nature **395**(6704), 777–780 (1998)
75. Khurana, K.K., Kivelson, M.G., Stevenson, D.J., Schubert, G., Russell, C.T., Walker, R.J., Polanskey, C.: Induced magnetic fields as evidence for subsurface oceans in Europa and Callisto **395**, 777–780 (1998)
76. Kimura, J., Nakagawa, T., Kurita, K.: Size and compositional constraints of Ganymede's metallic core for driving an active dynamo. Icarus **202**(1), 216–224 (2009)
77. Kirk, R., Stevenson, D.: Thermal evolution of a differentiated Ganymede and implications for surface features. Icarus **69**(1), 91–134 (1987)
78. Kirk, R.L., Stevenson, D.J.: Thermal evolution of a differentiated Ganymede and implications for surface features. Icarus **69**, 91–134 (1987). DOI 10.1016/0019-1035(87)90009-1
79. Kivelson, M., Khurana, K., Volwerk, M.: The permanent and inductive magnetic moments of Ganymede. Icarus **157**(2), 507–522 (2002)
80. Kivelson, M.G., Khurana, K.K., Stevenson, D.J., Bennett, L., Joy, S., Russell, C.T., Walker, R.J., Zimmer, C., Polanskey, C.: Europa and Callisto: Induced or intrinsic fields in a periodically varying plasma environment **104**(A3), 4609–4625 (1999)
81. Kivelson, M.G., Khurana, K.K., Volwerk, M.: The permanent and inductive magnetic moments of Ganymede **157**, 507–522 (2002)
82. Klotz, S., Bove, L., Strssle, T., Hansen, T., Saitta, A.: The preparation and structure of salty ice VII under pressure. Nature Materials **8**, 405–409 (2009). URL http://www.ncbi.nlm.nih.gov/entrez/query.fcgi?db=pubmedcmd=Retrievedopt=AbstractPluslist$_u ids = related : 7djwivm08nUJ$
83. Klotz, S., Komatsu, K., Kagi, H., Kunc, K., Sano-Furukawa, A., Machida, S., Hattori, T.: Bulk moduli and equations of state of ice VII and ice VIII. Physical Review B **95**(17), 174111 (2017). DOI 10.1103/PhysRevB.95.174111. URL https://link.aps.org/doi/10.1103/PhysRevB.95.174111
84. Kruijer, T.S., Burkhardt, C., Budde, G., Kleine, T.: Age of jupiter inferred from the distinct genetics and formation times of meteorites. Proceedings of the National Academy of Sciences **114**(26), 6712–6716 (2017)
85. Kuskov, O.L., Kronrod, V.A.: Core Sizes and Internal Structure of Earth's and Jupiter's Satellites. Icarus **151**, 204–227 (2001). DOI 10.1006/icar.2001.6611
86. Kuskov, O.L., Kronrod, V.A.: Internal structure of Europa and Callisto. Icarus **177**, 550–569 (2005). DOI 10.1016/j.icarus.2005.04.014
87. Lemasquerier, D., Grannan, A., Vidal, J., Cébron, D., Favier, B., Le Bars, M., Aurnou, J.: Libration-driven flows in ellipsoidal shells. Journal of Geophysical Research: Planets **122**(9), 1926–1950 (2017)
88. Malhotra, R.: Tidal origin of the Laplace resonance and the resurfacing of Ganymede. Icarus **94**, 399–412 (1991). DOI 10.1016/0019-1035(91)90237-N
89. Marounina, N., Grasset, O., Tobie, G., Carpy, S.: Role of the global water ocean on the evolution of Titan's primitive atmosphere. Icarus **310**, 127–139 (2018). DOI 10.1016/j.icarus.2017.10.048

90. McKinnon, W.: Core evolution in the icy galilean satellites, and the prospects for dynamo-generated magnetic fields. In: Bulletin of the American Astronomical Society, vol. 28, p. 1076 (1996)
91. McKinnon, W.B.: On convection in ice I shells of outer Solar System bodies, with detailed application to Callisto. Icarus **183**(2), 435–450 (2006). DOI 10.1016/j.icarus.2006.03.004. URL http://dx.doi.org/10.1016/j.icarus.2006.03.004
92. Millot, M., Coppari, F., Rygg, J.R., Barrios, A.C., Hamel, S., Swift, D.C., Eggert, J.H.: Nanosecond X-ray diffraction of shock-compressed superionic water ice. Nature **569**(7755), 251 (2019). DOI 10.1038/s41586-019-1114-6. URL https://www.nature.com/articles/s41586-019-1114-6
93. Mitri, G., Meriggiola, R., Hayes, A., Lefevre, A., Tobie, G., Genova, A., Lunine, J.I., Zebker, H.: Shape, topography, gravity anomalies and tidal deformation of Titan. Icarus **236**, 169–177 (2014). DOI 10.1016/j.icarus.2014.03.018. URL http://dx.doi.org/10.1016/j.icarus.2014.03.018
94. Monteux, J., Tobie, G., Choblet, G., Le Feuvre, M.: Can large icy moons accrete undifferentiated? Icarus **237**, 377–387 (2014). DOI 10.1016/j.icarus.2014.04.041
95. Morard, G., Andrault, D., Guignot, N., Sanloup, C., Mezouar, M., Petitgirard, S., Fiquet, G.: In situ determination of fe–fe$_3$s phase diagram and liquid structural properties up to 65 gpa. Earth and Planetary Science Letters **272**(3), 620–626 (2008)
96. Morard, G., Sanloup, C., Fiquet, G., Mezouar, M., Rey, N., Poloni, R., Beck, P.: Structure of eutectic fe–fes melts to pressures up to 17 gpa: implications for planetary cores. Earth and Planetary Science Letters **263**(1), 128–139 (2007)
97. Mosqueira, I., Estrada, P.R.: Formation of the regular satellites of giant planets in an extended gaseous nebula I: subnebula model and accretion of satellites. Icarus **163**, 198–231 (2003). DOI 10.1016/S0019-1035(03)00076-9
98. Mosqueira, I., Estrada, P.R.: Formation of the regular satellites of giant planets in an extended gaseous nebula II: satellite migration and survival. Icarus **163**, 232–255 (2003). DOI 10.1016/S0019-1035(03)00077-0
99. Nagel, K., Breuer, D., Spohn, T.: A model for the interior structure, evolution, and differentiation of Callisto. Icarus **169**, 402–412 (2004). DOI 10.1016/j.icarus.2003.12.019
100. Neubauer, F.M.: The sub-Alfvénic interaction of the Galilean satellites with the Jovian magnetosphere **103**(E9), 19843–19866 (1998)
101. Noack, L., Höning, D., Rivoldini, A., Heistracher, C., Zimov, N., Journaux, B., Lammer, H., Van Hoolst, T., Bredehöft, J.: Water-rich planets: How habitable is a water layer deeper than on earth? Icarus **277**, 215–236 (2016)
102. O'Rourke, J.G., Stevenson, D.J.: Stability of ice/rock mixtures with application to a partially differentiated Titan. Icarus **227**, 67–77 (2014). DOI 10.1016/j.icarus.2013.09.010
103. Pommier, A., Laurenz, V., Davies, C.J., Frost, D.J.: Melting phase relations in the fe-s and fe-so systems at core conditions in small terrestrial bodies. Icarus **306**, 150–162 (2018)
104. Ronnet, T., Mousis, O., Vernazza, P.: Pebble Accretion at the Origin of Water in Europa. Astropys. J. **845**, 92 (2017). DOI 10.3847/1538-4357/aa80e6

105. Rückriemen, T., Breuer, D., Spohn, T.: The fe-snow regime in ganymede's core: A deep-seated dynamo below a stable snow zone. Journal of Geophysical Research: Planets **497**, 365–380 (2015)
106. Rckriemen, T., Breuer, D., Spohn, T.: Top-down freezing in a fe-fes core and ganymede's present-day magnetic field. Icarus **307**, 172 – 196 (2018)
107. Sasaki, T., Stewart, G.R., Ida, S.: Origin of the Different Architectures of the Jovian and Saturnian Satellite Systems. ApJ **714**, 1052–1064 (2010). DOI 10.1088/0004-637X/714/2/1052
108. Saur, J., Duling, S., Roth, L., Jia, X., Strobel, D.F., Feldman, P.D., Christensen, U.R., Retherford, K.D., McGrath, M.A., Musacchio, F., Wennmacher, A., Neubauer, F.M., Simon, S., Hartkorn, O.: The search for a subsurface ocean in Ganymede with Hubble Space Telescope observations of its auroral ovals. Journal of Geophysical Research (Space Physics) **120**, 1715–1737 (2015). DOI 10.1002/2014JA020778
109. Saur, J., Neubauer, F.M., Glassmeier, K.H.: Induced magnetic fields in solar system bodies **152**, 391–421 (2010). DOI 10.1007/s11214-009-9581-y
110. Schilling, N., Neubauer, F.M., Saur, J.: Time-varying interaction of Europa with the jovian magnetosphere: Constraints on the conductivity of Europa's subsurface ocean **192**, 41–55 (2007)
111. Schubert, G., Anderson, J., Spohn, T., McKinnon, W.: Interior composition, structure and dynamics of the Galilean satellites. Jupiter: The Planet, Satellites and Magnetosphere pp. 281–306 (2004)
112. Schubert, G., Spohn, T., Reynolds, R.T.: Thermal histories, compositions and internal structures of the moons of the solar system. In: IAU Colloq. 77: Some Background about Satellites, pp. 224–292 (1986)
113. Scott, H., Williams, Q., Ryerson, F.: Experimental constraints on the chemical evolution of large icy satellites. Earth and Planetary Science Letters **203**(1), 399–412 (2002)
114. Shock, E.L., Holland, M.E.: Quantitative habitability. Astrobiology **7**(6), 839–851 (2007). DOI 10.1089/ast.2007.0137. URL http://dx.doi.org/10.1089/ast.2007.0137
115. Showman, A., Malhotra, R.: Tidal evolution into the laplace resonance and the resurfacing of ganymede. Icarus **127**(1), 93–111 (1997)
116. Showman, A.P., Malhotra, R.: Tidal Evolution into the Laplace Resonance and the Resurfacing of Ganymede. Icarus **127**, 93–111 (1997). DOI 10.1006/icar.1996.5669
117. Sohl, F., Choukroun, M., Kargel, J., Kimura, J., Pappalardo, R., Vance, S., Zolotov, M.: Subsurface Water Oceans on Icy Satellites: Chemical Composition and Exchange Processes. Space Science Reviews **153**, 485–510 (2010). DOI 10.1007/s11214-010-9646-y
118. Sohl, F., Sears, W.D., Lorenz, R.D.: Tidal dissipation on titan. Icarus **115**(2), 278–294 (1995)
119. Sohl, F., Spohn, T., Breuer, D., Nagel, K.: Implications from Galileo observations on the interior structure and chemistry of the Galilean satellites. Icarus **157**(1), 104–119 (2002)
120. Sotin, C., Gillet, P., Poirier, J.: Creep of high-pressure ice vi. In: Ices in the solar system, pp. 109–118. Springer (1985)
121. Sotin, C., Parmentier, E.: On the stability of a fluid layer containing a univariant phase transition: application to planetary interiors. Physics of

the Earth and Planetary Interiors **55**(1), 10–25 (1989). DOI 10.1016/0031-9201(89)90229-X
122. Sotin, C., Poirier, J.: Viscosity of ice v. Le Journal de Physique Colloques **48**(C1), 1–1 (1987)
123. Spohn, T., Breuer, D.: Interior structure and evolution of the galilean satellites. In: Planetary Systems: The Long View, p. 135 (1998)
124. Squyres, S.W., Reynolds, R.T., Summers, A.L., Shung, F.: Accretional heating of the satellites of Saturn and Uranus. J. Geophys. Res. **93**, 8779–8794 (1988). DOI 10.1029/JB093iB08p08779
125. Stevenson, D.J., Spohn, T., Schubert, G.: Magnetism and thermal evolution of the terrestrial planets. Icarus **54**(3), 466–489 (1983)
126. Tammann, G.: Ueber die Grenzen des festen Zustandes IV. Annalen der Physik **307**(5), 1–31 (1900). DOI 10.1002/andp.19003070502. URL https://onlinelibrary.wiley.com/doi/abs/10.1002/andp.19003070502
127. Tchijov, V.: Heat capacity of high-pressure ice polymorphs. Journal of Physics and Chemistry of Solids **65**(5), 851–854 (2004). DOI 10.1016/j.jpcs.2003.08.019. URL http://www.sciencedirect.com/science/article/pii/S0022369703003287
128. Tobie, G., Gautier, D., Hersant, F.: Titan's bulk composition constrained by cassini-huygens: Implication for internal outgassing. The Astrophysical Journal **752**(2), 125 (2012)
129. Tobie, G., Grasset, O., Lunine, J.I., Mocquet, A., Sotin, C.: Titan's internal structure inferred from a coupled thermal-orbital model. Icarus **175**(2), 496–502 (2005)
130. Tobie, G., Grasset, O., Lunine, J.I., Mocquet, A., Sotin, C.: Titan's internal structure inferred from a coupled thermal-orbital model. Icarus **175**, 496–502 (2005). DOI 10.1016/j.icarus.2004.12.007
131. Tobie, G., Lunine, J., Sotin, C.: Episodic outgassing as the origin of atmospheric methane on Titan. Nature **440**(7080), 61–4 (2006)
132. Tobie, G., Lunine, J.I., Monteux, J., Mousis, O., Nimmo, F.: The origin and evolution of Titan, p. 29 (2014)
133. Tobie, G., Lunine, J.I., Sotin, C.: Episodic outgassing as the origin of atmospheric methane on Titan. Nature **440**, 61–64 (2006). DOI 10.1038/nature04497
134. Tobie, G., Mocquet, A., Sotin, C.: Tidal dissipation within large icy satellites: Applications to Europa and Titan. Icarus **177**, 534–549 (2005). DOI 10.1016/j.icarus.2005.04.006
135. Vance, S., Bouffard, M., Choukroun, M., Sotin, C.: Ganymedes internal structure including thermodynamics of magnesium sulfate oceans in contact with ice. Planetary and Space Science **96**, 62–70 (2014). DOI 10.1016/j.pss.2014.03.011. URL http://dx.doi.org/10.1016/j.pss.2014.03.011
136. Vance, S., Bouffard, M., Choukroun, M., Sotin, C.: Ganymedes internal structure including thermodynamics of magnesium sulfate oceans in contact with ice. Planetary and Space Science **96**, 62–70 (2014). DOI 10.1016/j.pss.2014.03.011. URL http://www.sciencedirect.com/science/article/pii/S0032063314000695
137. Vance, S., Brown, J.M.: Thermodynamic properties of aqueous MgSO4 to 800 MPa at temperatures from - 20 to 100 C and concentrations to 2.5mol kg-1 from sound speeds, with applications to icy world oceans. Geochimica

et Cosmochimica Acta **110**, 176–189 (2013). DOI 10.1016/j.gca.2013.01.040. URL http://dx.doi.org/10.1016/j.gca.2013.01.040

138. Vance, S., Brown, J.M.: Thermodynamic properties of aqueous $MgSO_4$ to 800 MPa at temperatures from -20 to 100 ^oC and concentrations to 2.5 mol kg^{-1} from sound speeds, with applications to icy world oceans. Geochimica et Cosmochimica Acta **110**, 176–189 (2013). DOI 10.1016/j.gca.2013.01.040. URL http://dx.doi.org/10.1016/j.gca.2013.01.040
139. Vance, S., Harnmeijer, J., Kimura, J., Hussmann, H., deMartin, B., Brown, J.M.: Hydrothermal systems in small ocean planets. Astrobiology **7**(6), 987–1005 (2007). DOI 10.1089/ast.2007.0075. URL http://dx.doi.org/10.1089/ast.2007.0075
140. Vance, S.D., Hand, K.P., Pappalardo, R.T.: Geophysical controls of chemical disequilibria in Europa. Geophysical Research Letters **43**(10), 4871–4879 (2016)
141. Vance, S.D., Panning, M.P., Stähler, S., Cammarano, F., Bills, B.G., Tobie, G., Kamata, S., Kedar, S., Sotin, C., Pike, W.T., et al.: Geophysical investigations of habitability in ice-covered ocean worlds. Journal of Geophysical Research: Planets (2018). DOI 10.1002/2017je005341. URL http://dx.doi.org/10.1002/2017JE005341
142. Vance, S.D., Panning, M.P., Sthler, S., Cammarano, F., Bills, B.G., Tobie, G., Kamata, S., Kedar, S., Sotin, C., Pike, W.T., Lorenz, R., Huang, H.H., Jackson, J.M., Banerdt, B.: Geophysical Investigations of Habitability in Ice-Covered Ocean Worlds: GEOPHYSICAL HABITABILITY. Journal of Geophysical Research: Planets **123**(1), 180–205 (2018). DOI 10.1002/2017JE005341. URL http://doi.wiley.com/10.1002/2017JE005341
143. Wagner, W., Pru, A.: The IAPWS formulation 1995 for the thermodynamic properties of ordinary water substance for general and scientific use. Journal of Physical and Chemical Reference Data **31**(2), 387–535 (2002). URL http://scitation.aip.org/content/aip/journal/jpcrd/31/2/10.1063/1.1461829
144. Wagner, W., Riethmann, T., Feistel, R., Harvey, A.H.: New Equations for the Sublimation Pressure and Melting Pressure of H2o Ice Ih. Journal of Physical and Chemical Reference Data **40**(4), 043103 (2011). DOI 10.1063/1.3657937. URL https://aip.scitation.org/doi/abs/10.1063/1.3657937
145. Wagner, W., Riethmann, T., Feistel, R., Harvey, A.H.: New equations for the sublimation pressure and melting pressure of h2o ice ih. Journal of Physical and Chemical Reference Data **40**(4), 043103 (2011). DOI 10.1063/1.3657937
146. Wagner, W., Saul, A., Pruss, A.: International equations for the pressure along the melting and along the sublimation curve of ordinary water substance. Journal of Physical and Chemical Reference Data **23**(3), 515–527 (1994). DOI 10.1063/1.555947
147. Williams, Q.: Bottom-up versus top-down solidification of the cores of small solar system bodies: Constraints on paradoxical cores. Earth and Planetary Science Letters **284**(3), 564–569 (2009)
148. Yoshino, T., Walter, M.J., Katsura, T.: Core formation in planetesimals triggered by permeable flow. Nature **422**(6928), 154 (2003)
149. Zhan, X., Schubert, G.: Powering ganymede's dynamo. Journal of Geophysical Research **117**(E8), E08011 (2012)
150. Zimmer, C., Khurana, K., Kivelson, M.: Subsurface oceans on Europa and Callisto: Constraints from Galileo magnetometer observations **147**, 329–347

(2000)
151. Zimmer, C., Khurana, K.K., Kivelson, M.G.: Subsurface oceans on Europa and Callisto: Constraints from Galileo magnetometer observations. Icarus **147**(2), 329–347 (2000)
152. Zolotov, M.Y.: Oceanic Composition on Europa: Constraints from Mineral Solubilities. Lunar and Planetary Institute Science Conference Abstracts **39**, 2349 (2008). URL http://adsabs.harvard.edu/abs/2008LPI....39.2349Z